Timescale for Detecting the Climate Response to Stratospheric Aerosol Geoengineering

Douglas G. MacMartin[1], Wenli Wang[2], Ben Kravitz[3], Simone Tilmes[4], Jadwiga H. Richter[5], and Michael J. Mills[4]

[1]Mechanical and Aerospace Engineering, Cornell University, Ithaca, NY, USA, [2]College of Global Change and Earth System Science, Beijing Normal University, Beijing, China, [3]Atmospheric Sciences and Global Change Division, Pacific Northwest National Laboratory, Richland, WA, USA, [4]Atmospheric Chemistry, Observations, and Modeling Laboratory, National Center for Atmospheric Research, Boulder, CO, USA, [5]Climate and Global Dynamics Laboratory, National Center for Atmospheric Research, Boulder, CO, USA

Abstract Stratospheric aerosol geoengineering could be used to maintain global mean temperature despite increased atmospheric greenhouse gas (GHG) concentrations, for example, to meet a 1.5 or 2 °C target. While this might reduce many climate change impacts, the resulting climate would not be the same as one with the same global mean temperature due to lower GHG concentrations. The primary question we consider is how long it would take to detect these differences in a hypothetical deployment. We use a 20-member ensemble of stratospheric sulfate aerosol geoengineering simulations in which SO_2 is injected at four different latitudes to maintain not just the global mean temperature, but also the interhemispheric and equator-to-pole gradients. This multiple-latitude strategy better matches the climate changes from increased GHG, while the ensemble allows us both to estimate residual differences even when they are small compared to natural variability and to estimate the statistics of variability. We first construct a linear emulator to predict the model responses for different scenarios. Under an RCP4.5 scenario in which geoengineering maintains a 1.5 °C target (providing end-of-century cooling of 1.7 °C), the projected changes in temperature, precipitation, and precipitation minus evaporation (P − E) at a grid-scale are typically small enough that in many regions the signal-to-noise ratio is still less than one at the end of this century; for example, for P − E, only 30% of the land area reaches a signal-to-noise ratio of one. These results provide some context for the projected magnitude of climate changes associated with a limited deployment of stratospheric aerosol cooling.

Plain Language Summary Stratospheric aerosol geoengineering could be used to maintain global mean temperature in the presence of increased atmospheric greenhouse gas concentrations, for example, to meet the 1.5 or 2 °C targets from the Paris agreement. While this might reduce many climate change impacts, the resulting climate would not be the same as one where the same global mean temperature was achieved due to lower greenhouse gas concentrations. An important factor in evaluating geoengineering is understanding how different these climates might be? To provide context for these differences, we evaluate how long it would take to detect that the geoengineered climate was different. For moderate deployment scenarios, changes in regional temperature and precipitation patterns would not be detectable over much of the planet even by the end of this century.

1. Introduction

Stratospheric aerosol geoengineering could be considered as part of a portfolio of options for managing future climate change (Crutzen, 2006; Keith & MacMartin, 2015; Long & Shepherd, 2014; MacMartin et al., 2018; Wigley, 2006) and could reduce many impacts relative to the warmer world without geoengineering (e.g., Keith & Irvine, 2016). However, while geoengineering could be used to maintain some particular target for global mean temperature, such as a 1.5 or 2 °C rise above preindustrial levels, the resulting climate would not be the same as one in which these targets were achieved solely through limiting atmospheric greenhouse gas (GHG) concentrations (e.g., Jones et al., 2018; MacMartin et al., 2018).

One way of providing context for these differences is to compare them to the magnitude of interannual natural variability in the climate system; similar analysis has been conducted for climate change, for example, by

Hawkins and Sutton (2012) or Frame et al. (2017). A closely related question is, for any particular scenario, how long would it take to detect that the climate had changed? The answers to these questions are important not only for providing a contextual understanding of projected climate differences that can ultimately feed in to future decisions about this technology, but also for input into more formal detection and attribution studies and the associated construction of governance regimes. Previous analyses (Bürger & Cubasch, 2015; Lo et al., 2016) have focused on detecting large-scale and global changes relative to the continually increasing temperatures that would have occurred without geoengineering; here we consider the challenge of detecting changes at the regional and model grid-scale caused by how geoengineering affects the climate differently from changes in GHG concentrations.

We estimate the climate response to stratospheric aerosol geoengineering and the resulting detection timescales using simulations from the Geoengineering Large Ensemble Project (GLENS), described by Tilmes, Richter, Kravitz, et al. (2018). These simulations include three features that are important here.

First, this is the first large ensemble conducted for evaluating geoengineering. Using a 20-member ensemble allows us to more accurately identify the forced response and distinguish it from variability. We also use the spread across the ensemble to estimate the statistics of variability for comparison (similar to Deser et al., 2012; Kay et al., 2015).

Second, the climate model used (Mills et al., 2016; Mills et al., 2017, see section 2) includes a number of important stratospheric processes that have not all been included in past geoengineering simulations (see e.g., Table 2 in Pitari et al., 2014) but are important for capturing the climate response to SO_2 injection. These include a model of aerosol microphysical processes, stratospheric chemistry including ozone, and sufficient spatial resolution to capture potential dynamic influences on stratospheric circulation including changes to the quasi-biennial oscillation (Aquila et al., 2014; Richter et al., 2017, 2018).

And third, most previous simulations of stratospheric aerosol geoengineering have chosen equatorial or tropical injection (e.g., Kalidindi et al., 2015; Niemeier & Timmreck, 2015; Pitari et al., 2014). This produces a peak in aerosol optical depth in the tropics, leading to an overcooling of the tropics and undercooling of the poles, the same dominant temperature pattern observed in simulations of a solar reduction (Kravitz et al., 2013). However, because the response will depend on choices such as the injection latitude(s), it is essential to evaluate the climate response to geoengineering in the context of an intentionally designed rather than ad hoc strategy (Kravitz et al., 2016). The GLENS simulations thus inject SO_2 (which forms sulfate aerosols) at four different latitudes identified by Tilmes et al. (2017) and MacMartin et al. (2017) to simultaneously maintain not just the global mean temperature (T0) but also the interhemispheric temperature gradient (T1) and equator-to-pole gradient (T2). A feedback algorithm adjusts the injection rates each year as necessary to maintain these goals (Kravitz et al., 2017). A strategy that did not maintain T1 could lead to significant shifts in tropical precipitation (Haywood et al., 2013), while controlling for T2 reduces the tendency to overcool the tropics relative to poles. This strategy thus leads to a better compensation of GHG-induced climate change than equatorial-only injection strategies (MacMartin et al., 2017). Nonetheless, it is not based on an exhaustive exploration of all possible deployment design choices. Thus, residual differences (relative to a lower GHG world with the same global mean temperature) should not be interpreted as unavoidable consequences of any geoengineering strategy but rather as motivation for further research to explore alternate strategies, much as the overcooled tropics in previous simulations motivates strategies to manage T2 in addition to T0.

One important feature that is not included herein is a comparison of the response across different models as in the Geoengineering Model Intercomparison Project (Kravitz et al., 2013; MacMartin et al., 2018). However, similar simulations have not yet been conducted with any other model.

The GLENS simulations were conducted with a Representative Concentration Pathway RCP8.5 emissions scenario (Meinshausen et al., 2011) and sufficient stratospheric sulfate aerosol geoengineering to maintain the global mean temperature T0 as well as the gradients T1 and T2 near their 2020 levels. Detection depends on the ratio of the forced response (the "signal") to the natural climate variability (the "noise"); the timescale thus depends on the specific scenario and in particular how much cooling is provided by the geoengineering. It is valuable to consider different possible future emissions-pathways and temperature targets, including limited deployment scenarios to limit warming in the presence of more stringent mitigation efforts than that of RCP8.5. For example, mitigation commitments made under the 2015 Paris Agreement may lead to of

order 3 °C warming (Rogelj et al., 2016), which is more consistent with an RCP4.5 scenario, while the Paris Agreement also defined targets of 2 °C and ideally no more than 1.5 °C increase in global mean temperature above preindustrial.

In order to estimate how this climate model would have responded to different scenarios involving different levels of emissions or different targets for the geoengineered global mean temperature, we first construct a linear dynamic emulator following MacMartin and Kravitz (2016), using a semi-infinite-diffusion model to capture the change in global mean temperature (see also Caldeira & Myhrvold, 2013; MacMynowski et al., 2011; MacMartin et al., 2018) and pattern scaling (Mitchell, 2003; Santer et al., 1990; Tebaldi & Arblaster, 2014) to describe the projected spatial patterns of response. Despite using three objectives (T0, T1, T2) to determine the amount of SO_2 to inject at different latitudes, the response pattern for geoengineering can still be scaled in terms of a single number, the change in global mean temperature; the changes in T1 and T2 due to geoengineering will then scale with the change in T0. This is a reasonable choice as the changes in T1 and T2 due to increased GHG concentrations are also proportional to the change in global mean temperature, so that scaling the geoengineering response to meet a target global mean temperature means that the values of the interhemispheric and equator-to-pole gradients T1 and T2 will also be maintained at values consistent with the global mean temperature T0.

We apply this emulator herein for changes in annual-mean surface air temperature, precipitation, and precipitation minus evaporation (P − E). Changes in P − E are more relevant to assessing impacts of hydrological cycle changes than annual-mean precipitation; we include precipitation both because it has frequently been considered in past analyses and because in the specific context of detection, it would be a straightforward variable to observe. The same approach could be used to consider additional climate variables relevant for assessing climate impacts, although the approach will not work as well for some fields such as stratospheric ozone, where the response also depends on time-varying stratospheric concentrations of ozone depleting substances. In this model, the assumption of linearity is reasonable for the variables considered here and for at least a few degrees of cooling (section 3, see also Kravitz et al., 2017; MacMartin et al., 2017). At higher cooling levels, nonlinearities in aerosol microphysics are expected to result in greater injection rates being needed per unit cooling (English et al., 2012; Heckendorn et al., 2009; Kleinschmitt et al., 2018; Niemeier & Timmreck, 2015; Pierce et al., 2010), which could be expected to have nonlinear influences on surface climate.

Section 2 describes the GLENS simulations in more detail and section 3 describes the construction and validation of the emulator, including the (scaled) spatial pattern of response per degree of GHG warming and the (scaled) spatial pattern of response per degree of stratospheric aerosol cooling. Section 4 then compares the estimated difference in response with the magnitude of natural variability, both to provide context for how important some of the regional changes might be and to assess for particular scenarios the time it would take before the "signal" from the geoengineering deployment could be detected in the presence of the noise from background variability.

2. Simulations

The GLENS simulations are described in detail by Tilmes, Richter, Kravitz, et al. (2018). Simulations were conducted with the Community Earth System Model version 1, with the Whole Atmosphere Community Climate Model as its atmospheric component, CESM1(WACCM). The model resolution is 0.9° in latitude by 1.25° in longitude, with 70 vertical layers in the atmosphere up to 140 km in order to capture the entire stratosphere. The model description and validation are given by Mills et al. (2017), with the exception that the version used here has a different land model as described by Tilmes, Richter, Kravitz, et al. (2018). The model includes oxidation of SO_2 to H_2SO_4 and includes a modal description of sulfate aerosol microphysics (Liu et al., 2012) to represent nucleation, condensation, coagulation, evaporation, and sedimentation processes; the modal description is a compromise choice between computation and fidelity and may limit the ability to capture the aerosol size distribution. The model also includes interactive stratospheric chemistry and dynamics, both of which can alter the stratospheric circulation (Richter et al., 2017; 2018) and thus influence aerosol spatial distributions as well as directly influencing the tropospheric response (e.g., Driscoll et al., 2012). The model is fully coupled to land, ocean, and sea ice components.

All of the GLENS simulations use prescribed emissions following the Representative Concentration Pathway RCP8.5 pathway (Meinshausen et al., 2011). A 20-member ensemble of RCP8.5 simulations was conducted
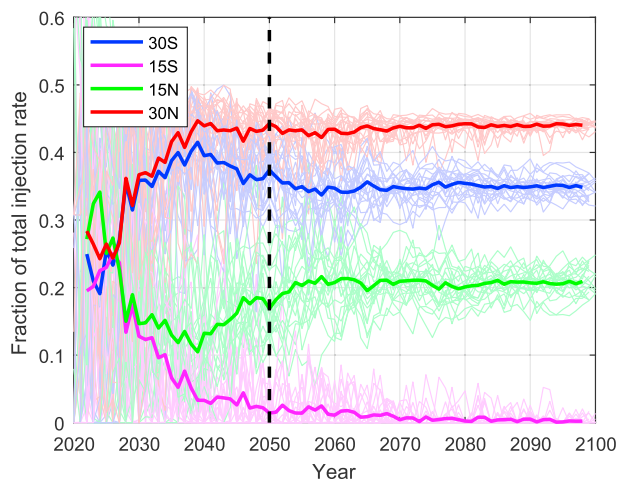
Figure 1. Fraction of injection applied at each of four latitudes throughout the simulation; individual simulations in light colors and ensemble mean in solid. The initial estimate for the fraction of injection at each latitude required to meet temperature goals was gradually corrected in the initial decades using feedback of the actual climate response. The pattern of response to stratospheric aerosol geoengineering is estimated using years after 2050 (shown with vertical dashed line) when the distribution of injection has (mostly) converged.

from 2010–2030, with three ensemble members extended until 2097. The average of these simulations over the 2010–2030 period is taken as the reference period in subsequent analyses; using 21×20 years means that the reference climate in this model is known to an accuracy of order a factor of 20 times smaller than the standard deviation of variability. The 20-member ensemble of geoengineering simulations were branched from the RCP8.5 simulations in 2020 and continued until 2099.

Rather than injecting SO_2 at only one latitude, as has typically been done in many prior geoengineering simulations, SO_2 was injected at four different latitudes simultaneously; 15°S and 15°N at 25 km altitude and 30°S and 30°N at 22.8 km, all at 180°E. These were identified by Tilmes et al. (2017) and MacMartin et al. (2017) to enable independent control over three different spatial distributions of aerosol optical depth; similar conclusions have been found independently in a different model (Dai et al., 2018). As in Kravitz et al. (2016; 2017), the goal chosen for the simulations was to simultaneously maintain the global mean temperature (T0), the interhemispheric temperature gradient (T1), and the equator-to-pole temperature gradient (T2) at 2020 levels. An initial estimate was made for the required injection rates at each latitude, and then in each year of the simulation, these injection rates were adjusted as necessary using a feedback algorithm, described by Kravitz et al. (2017). The feedback approach ensures that the goals are met despite some uncertainty and nonlinearity in the system. The strategy of managing multiple degrees of freedom allows for a better compensation of surface temperature patterns (Mac-Martin et al., 2017), in particular reducing the tendency in past geoengineering simulations of overcooling the tropics and undercooling the poles (e.g., Kravitz et al., 2013). Other design variables such as different altitudes (Tilmes, Richter, Mills, et al., 2018), aerosols (Keith et al., 2016), or injecting as H_2SO_4 rather than SO_2 (to yield smaller sulfate aerosols; Benduhn et al., 2016; Pierce et al., 2010) would yield different climate responses even for meeting the same climate objectives.

The initial estimates for injection rates were derived from a single previous simulation (Kravitz et al., 2017) that was conducted with the previous version of the land model. These estimates were not quite sufficient to manage the interhemispheric gradient, and during the first ~20 years of the simulation the feedback algorithm correctly converged to the pattern of injection needed to meet the temperature goals (Figure 1; see also Figure 2 in Tilmes, Richter, Kravitz, et al., 2018). This means that the relative distribution of injection across the four latitudes in the early part of the simulation differs from the relative distribution in later decades, and as a result the spatial pattern of response differs slightly. This influences our choice of methodology for defining the characteristic spatial response pattern as described in section 3.2 below.

The use of a feedback algorithm to adjust the injection rates will also affect the statistics of climate variability, described in detail by MacMartin et al. (2014). The algorithm reacts to differences in T0, T1, and T2 relative to their target values regardless of whether those differences are due to incorrect estimates for the injection rates or due to natural variability. As a result, the algorithm will suppress variability in T0, T1, and T2 at timescales longer than the convergence time of the algorithm (chosen here to be roughly 5 years), and this may affect variability in other variables as well. In addition, there will be some amplification of variability in T0, T1, and T2 at timescales commensurate with the convergence time (see; MacMartin et al., 2014). We estimate the detection timescales in section 4.2 using natural variability statistics estimated from these feedback-geoengineered simulations.
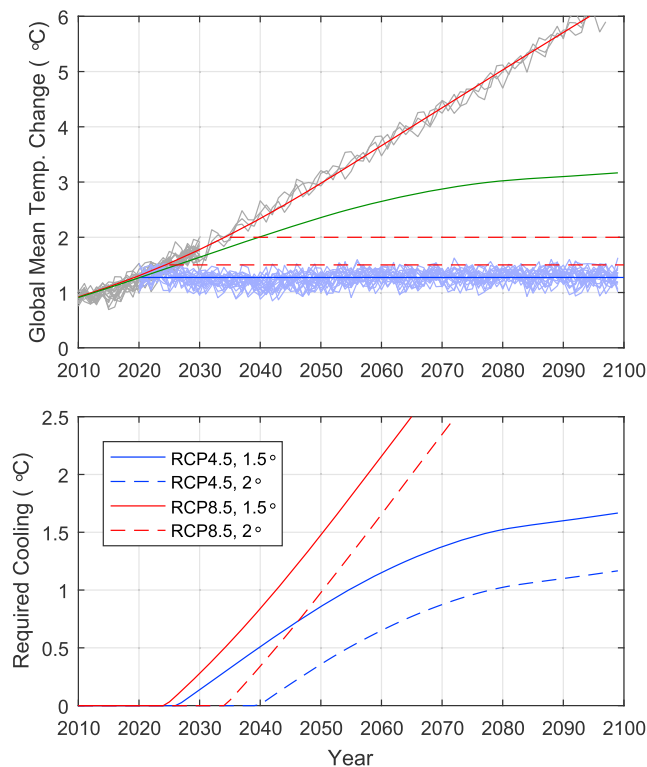
The global mean temperature in the simulations is shown in Figure 2a, described in section 3 below.

3. Emulator and Pattern Scaling

Section 4 considers several possible future scenarios, such as following a RCP4.5 trajectory of GHG concentrations, with sufficient stratospheric aerosol geoengineering to maintain global mean temperature at the Paris Agreement target of 1.5 °C. In order to estimate the projected climate response to alternate scenarios such as this without having to run new simulations for each possible scenario, it is useful to develop

Figure 2. (a) Global mean temperature; individual simulations shown in light gray (RCP8.5 without geoengineering) or blue (with geoengineering), along with the target value for geoengineering (dark blue line) and the fit of the RCP8.5-only ensemble mean to a semi-infinite diffusion model (red line); also shown is the resulting projected model response to an RCP4.5 scenario without geoengineering (green line). The temperature is defined so that the average over 2006–2015 is 0.87 °C, consistent with IPCC usage so that the Paris targets of 1.5 and 2 °C (dashed red lines) are defined relative to this value. (b) Difference, in degrees, between model-projected global mean temperature change for the RCP4.5 or RCP8.5 scenarios and 1.5 or 2 °C temperature targets, representing the amount of cooling that would need to be provided by geoengineering to maintain these targets.

an emulator for the model response. There are two components to this emulator. First, a dynamic model is used to predict the time-varying global mean temperature response for any time-dependent pathway of GHG forcing and any level of geoengineering. Second, the response of any other variable (such as the temperature or precipitation at each grid cell) is assumed to scale proportionally with changes in the global mean temperature. This pattern-scaling approach has been used extensively, both for climate change alone (e.g., Mitchell, 2003; Santer et al., 1990; Tebaldi & Arblaster, 2014) and for geoengineering (MacMartin & Kravitz, 2016; MacMartin et al., 2018). We only include a single response pattern here for each variable; this assumes that all of the dynamics that capture the memory of past forcing can be described by a single number, the global mean temperature. Additional spatial patterns with additional predictive variables could be included to capture differences in the short-term and long-term response as in Joshi et al. (2013), Holden and Edwards (2010), Castruccio et al. (2014), or MacMartin and Kravitz (2016). However, for gradually varying forcing, a single spatial pattern, scaled with the change in global mean temperature, captures most of the forced response (this is validated below in Figure 4).

3.1. Dynamics

The global mean temperature response to either GHG forcing or a solar reduction can be well approximated by the response to a semi-infinite diffusion model as in MacMynowski et al. (2011) or Caldeira and Myhrvold (2013); see also MacMartin et al., (2018). With this assumption, the global mean temperature response to a unit step change in the forcing at $t = 0$ is given by

$$g(t) = \mu \left(1 - e^{t/\tau}\mathrm{erfc}(\sqrt{t/\tau})\right), \qquad (1)$$

where τ has units of time, μ is proportional to the climate sensitivity, and erfc is the complementary error function (and $g(t) = 0$ for $t \leq 0$). This functional form could be used directly to fit the model output from an abrupt $4 \times CO_2$ simulation, for example. The global-mean-temperature response to any other forcing trajectory $f(t)$ can be estimated using convolution. We approximate the forcing f as constant over any year and compute the annual-mean global mean temperature over year k as

$$T(k) = \sum_{j=0}^{j=k} h(k - j)f(j), \qquad (2)$$

where the discrete-time impulse response $h(k)$ can be calculated from the annually averaged step response as

$$h(k) = \int_{k}^{k+1} [g(t) - g(t - 1)]\mathrm{d}t. \qquad (3)$$

The best-fit parameter $\mu = 1.12$ °C/(W/m^2) for this model is estimated using a least-squares fit to the simulated response of CESM1(WACCM) to RCP8.5 forcing without geoengineering, with the forcing $f(t)$ estimated from the log of the CO_2-equivalent concentration; this corresponds to a climate sensitivity of 4.15 °C for a doubling of CO_2, higher than the current best estimate. Because the response to this slowly varying forcing is not strongly dependent on the timescale of the diffusion model, we use the value of $\tau = 7.2$ years that was estimated for CESM from its response to an abrupt $4 \times CO_2$ simulation (see supporting information for MacMartin et al., 2018); the emulated response to RCP4.5 is similarly not strongly dependent on this choice. Different climate models will have different sensitivity parameter μ and different timescale τ.

The resulting fit to the simulated temperature is shown in Figure 2a, illustrating that this two-parameter semi-infinite diffusion model is consistent with the climate model behavior. Also shown in Figure 2a is the
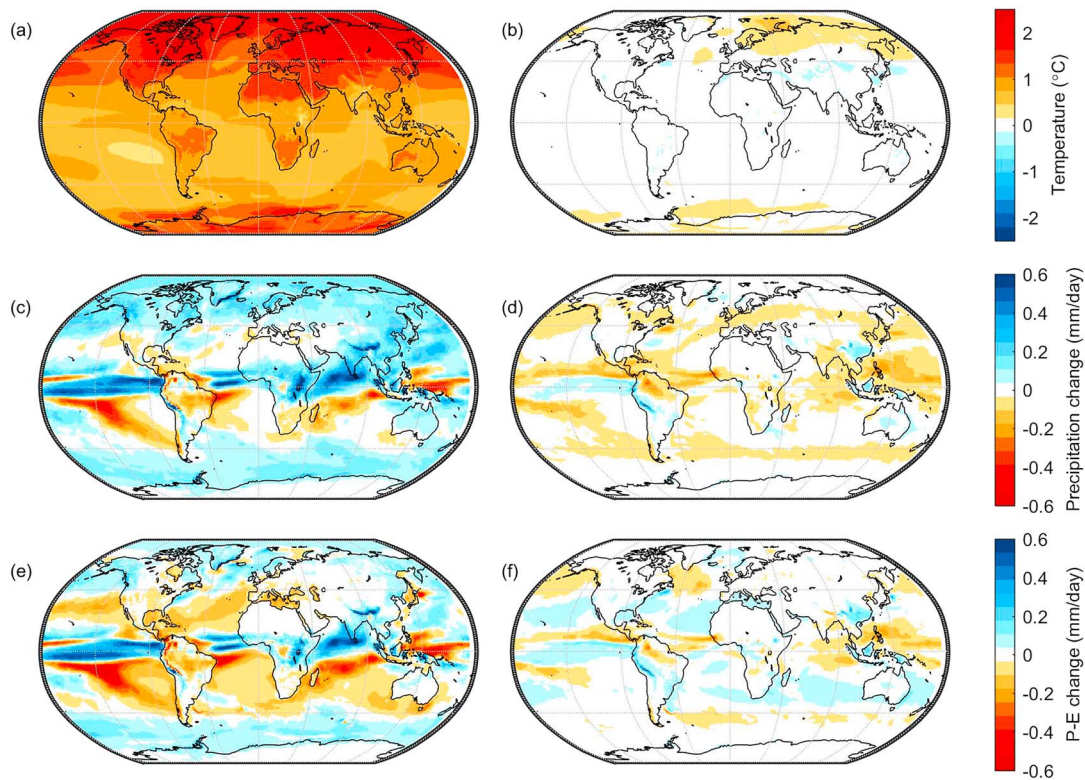
Figure 3. Climate response pattern to greenhouse gas forcing alone (a, c, e) and to the difference between GHG forcing and stratospheric sulfate aerosol geoengineering (b, d, f), for surface air temperature (a, b, degrees Celsius), precipitation (c, d; mm/day), and precipitation minus evaporation or P − E (e, f; mm/day). All changes are normalized per degree C change in global mean temperature (per degree C warming in the GHG case, and per degree C of GHG warming offset by the same amount of cooling in the geoengineered case, so panel (b) has zero global mean by construction.

predicted response of this model to an RCP4.5 scenario, obtained using equation (2); this assumes that the climate model response is linear (i.e., that μ and τ are not dependent on the level of forcing). In order to compare with policy-relevant targets for global mean temperature such as 1.5 or 2 °C, the temperature axis is adjusted so that the average temperature over the decade 2006–2015 is 0.87 °C, consistent with the observed temperature rise relative to preindustrial (Intergovernmental panel on climate change (IPCC), 2018). Also shown in Figure 2b is the amount of geoengineering needed to maintain a 1.5 or 2 °C target, measured in terms of the global cooling required (because of the higher climate sensitivity, this model predicts an earlier reaching of these targets than the best current estimate).

3.2. Pattern Scaling

The climate response corresponding to any particular scenario could be estimated as the (linear) sum of the responses to increased GHG forcing and to the stratospheric aerosol geoengineering. Instead, we equivalently describe the response as the sum of (a) the response to GHG forcing for the *actual* global mean temperature change after geoengineering (e.g., 1.5 or 2 °C), T, plus (b) a term that is proportional to the amount of geoengineered cooling provided, ΔT, that describes how the climate responds *differently* to geoengineering relative to GHG forcing (i.e., to the sum of positive GHG forcing and negative geoengineered forcing to yield zero global mean temperature change). The projected change in any variable $y(t)$ (e.g., the temperature at a single grid point) is thus assumed to be of the form

$$y = \alpha T + \beta \cdot \Delta T, \tag{4}$$

where $T + \Delta T$ is the temperature that would have occurred without any geoengineering, T is the actual temperature change due to the combination of increased GHG and geoengineering, α describes the response of variable y to increased GHG, while β describes the response of variable y to an increase in GHG that is offset by stratospheric aerosol cooling. We estimate both α and β below for a few different variables (shown in Figure 3) from the RCP8.5 and geoengineering simulations, the latter term is the primary focus of analysis in subsequent sections. We could instead consider $y = \alpha(T + \Delta T) + \mu \cdot \Delta T$, however, $\beta = \mu - \alpha$
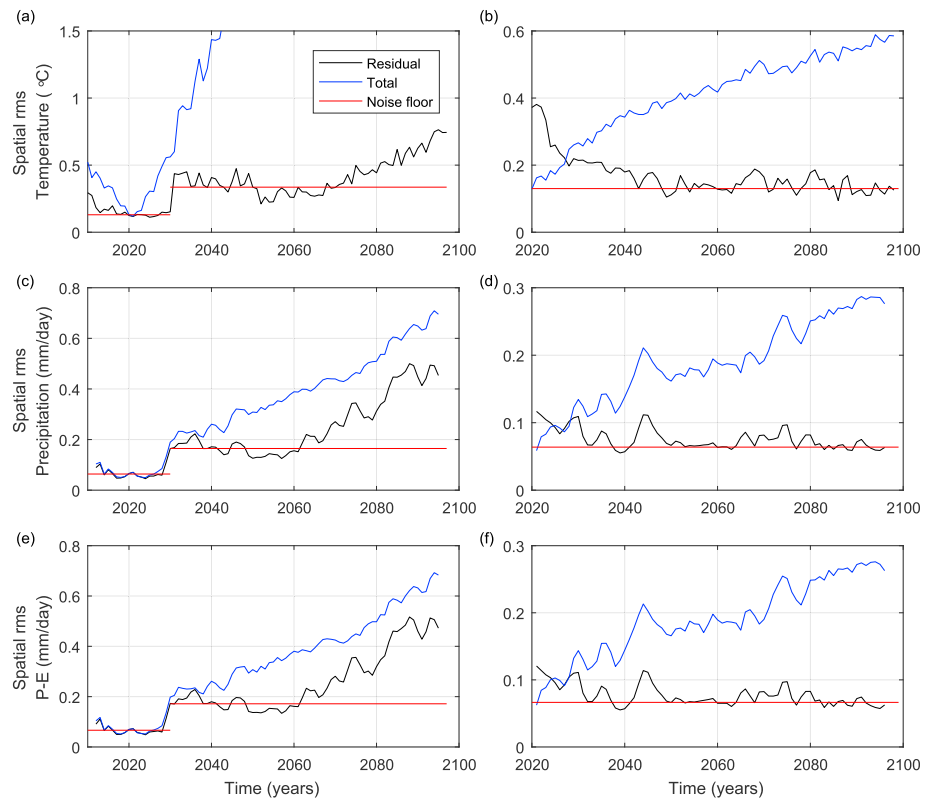
Figure 4. Spatial rms versus time illustrating that a single spatial pattern of change is sufficient to capture most of the forced response in this model. Panels are ordered as in Figure 3. For each case the rms residual is plotted (black; simulation minus the linear prediction), compared with the rms difference of the ensemble-mean relative to the reference period 2010–2030 (blue), and compared with the standard error due to natural variability (red; standard deviation divided by square root of number of ensemble members; for the RCP8.5 cases without geoengineering, the number of members is 20 from 2010–2030 and 3 thereafter). The precipitation and P − E are first smoothed with 5-year running means in this figure; otherwise the variability in these variables is almost as large as the forced response. rms = root-mean-square.

can be directly estimated from the constant-temperature geoengineering simulations, whereas to estimate μ we would need to difference the geoengineering and nongeoengineered simulations, unnecessarily introducing extra variability and potential nonlinearities.

Following equation (4), the response of any variable y to GHG forcing alone can be estimated from the ensemble mean of the RCP8.5 simulations using linear regression, where both y and T describe the departures from the 2010–2030 reference period mean value. For T here we use the value obtained from the semi-infinite diffusion fit as our best estimate for the global mean temperature response to the forcing; this is approximately equivalent to using the smoothed ensemble-mean temperature. This regression approach neglects nonlinearities in the climate response. At higher global-mean temperature, the departure from a linear assumption becomes larger in the Arctic in particular (see Figure S1); this is likely due at least in part to changes in the strength of sea ice feedback with decreasing ice extent. To better predict responses for the range of global-mean temperature changes consistent with an RCP4.5 scenario, we thus limit the regression to the period 2010–2060. As shown in Figure 4, for temperature, precipitation, and P − E considered here, the regression approach yields a reasonable predictive approximation over this time period, and nonlinearities become significant beyond it. The spatial root-mean-square of the residual error after subtracting out this single spatial pattern is similar to the limit one would expect from natural variability. (The estimated magnitude of natural variability is described in section 4 below.)

Estimating how this climate model responds differently to stratospheric aerosol geoengineering as compared with GHG forcing is similar with one modification. The relative distribution of SO_2 injection rates across the four injection latitudes converges by roughly 2050. Because the injection pattern differs during this transient, the climate response pattern also differs. As a result, we estimate the response pattern from
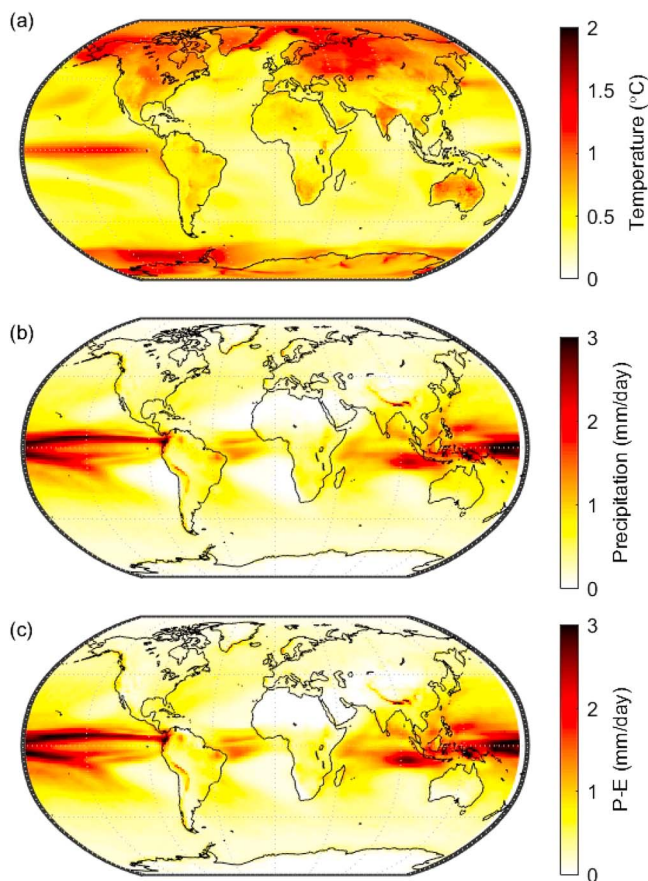
Figure 5. Standard deviation of interannual natural variability in this climate model estimated from all 20 ensemble members and years 2015–2030 of the no-geoengineering reference period, for surface air temperature (a), precipitation (b), and P − E (c).

the geoengineering simulations using only the time interval from 2050 through 2099, capturing the geoengineered pattern after convergence rather than before. For any variable y, the estimated functional form over the 2050–2099 time interval is of the form $y = \beta \cdot \Delta T + \gamma$, where the least-squares intercept $\gamma \neq 0$ due to the different initial pattern and β describes the post-convergence climate (roughly linear) response to increased levels of GHG that are offset by stratospheric aerosol cooling. Because the global mean temperature remains lower in the geoengineering simulations, the Arctic nonlinearities apparent by mid-century in the RCP8.5 scenario are not significant here, and there is no reason not to include later years in estimating the characteristic pattern of response. Figure 4 illustrates that for the variables considered here, predicting the behavior of this climate model to stratospheric aerosol geoengineering using only a single spatial pattern of response is a reasonable approximation, with the residual error again similar to what one would expect from natural variability. Despite using only the post-convergence years 2050–2099 in estimating the pattern of response per degree of cooling, the pattern-scaling prediction is reasonably similar to the simulated response except in the initial decade.

Different time periods are used in estimating the coefficients α and β from the no-geoengineering and geoengineering simulations, respectively; in each case the time period is chosen based on what is most representative for projecting the response to a lower emissions scenario.

The estimated response patterns are shown in Figure 3. These are normalized, for the GHG forcing, per degree of increase in global mean temperature, and for the stratospheric aerosol geoengineering forcing, per degree of cooling provided. The temperature pattern is consistent with that shown in Figure 6 of Tilmes, Richter, Kravitz, et al. (2018) and the P − E pattern consistent with Figure 2 of Fasullo et al. (2018). One of the dominant features in the geoengineered case is residual higher temperatures relative to the baseline period (still significantly cooler relative to the nongeoengineered case) at high-latitudes. This is likely a result of dynamic effects caused by the stratospheric aerosol-heating (Driscoll et al., 2012). The largest temperature changes are in places (e.g., Barents-Kara Sea and Sea of Okhotsk) where this leads to a loss of sea ice in the geoengineered case relative to baseline (this is more apparent in Figure 6). Precipitation and P − E shown here are in absolute units; the percentage change in each variable is shown in Figure S2.

The patterns in Figure 3 can be used to project how this model might respond to different future scenarios. Thus, for example, one could compare

(i) a world where 1.5 °C was obtained without the use of geoengineering (1.5 times the first column of Figure 3),
(ii) a world where mitigation was only sufficient to give 3 °C of warming without geoengineering (adding to case (i) an additional 1.5 times the first column), or
(iii) this same higher CO_2 level but with 1.5 °C cooling via stratospheric aerosols (adding to case (i) 1.5 times the second column instead).

This comparison is illustrated in Figure S3. Consistent with MacMartin et al., (2018) where a similar question was considered using simulations of a solar reduction, it is clear from Figure 3 that while case (iii) would differ from case (i), those differences would be small compared with the differences between either of those cases and the 3° case (ii). It is unclear whether a choice to use geoengineering would also influence the amount of mitigation. Future decisions may be influenced both by the comparison of the same
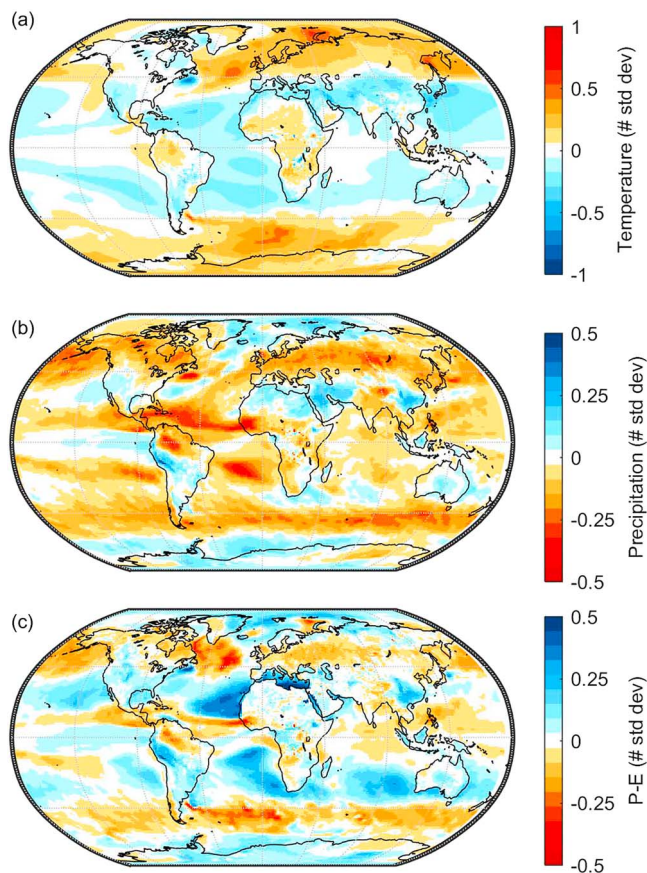
Figure 6. Response of annual-mean (a) temperature, (b) precipitation, and (c) P − E per degree Celsius of GHG warming that is offset by stratospheric aerosol geoengineering as in Figures 3b, 3d, and 3f, but here normalized by the results in Figure 5 to show the magnitude of change in units of standard deviations of interannual natural variability per degree Celsius of ΔT.

future emissions with and without geoengineering, and also by how geoengineering would affect the climate differently for the same global mean temperature.

4. Climate Variability and Detection Timescale

One approach for putting the magnitude of climate changes in context is to compare them with the magnitude of natural variability; this approach has been used both in assessing climate change (e.g., Frame et al., 2017; Hawkins & Sutton, 2012) as well as some past assessments of geoengineering (e.g., Kravitz et al., 2014; Ricke et al., 2010). One rationale for this is that a particular magnitude of change is potentially more important in a place that has not adapted to large year-to-year variations than it would be in a place where large variations are normal.

The second reason to compare the magnitude of changes with natural variability relates to detection time. Presumably, if it is difficult to detect a change in the presence of natural variability, then that change is likely to be less important. The time to detect changes is also important in understanding requirements for responsible governance. For different scenarios, we evaluate how long it would take for an observer, knowing how much geoengineering was being applied, to detect a change; that is, when their best observationally based estimate of the signal from the geoengineering deployment would exceed the noise from natural variability with some threshold. The baseline for this comparison is the climate corresponding to the same global-mean-temperature with lower levels of GHG and without geoengineering; for a scenario in which the temperature is held fixed at the level when geoengineering is started, this is roughly the same as comparing with the last historical period prior to the beginning of deployment.

4.1. Comparison With Variability

For consistency we estimate the statistics of interannual natural variability from the same ensemble; one caveat is that the statistics of variability in this model will differ from those in the real-world (as will the forced response). The interannual natural variability in Figure 5 is estimated from the RCP8.5 simulations without geoengineering; the variance estimated from the geoengineering simulations is similar. Because all simulations were initialized in 2010 with only small perturbations relative to the same atmospheric state, the ensemble members will be initially correlated with each other, and we estimate variability using only the period 2015–2030 after the ensemble-variance has converged. After subtracting the ensemble mean in each year from each of 20 ensemble members, this gives 19×16 degrees of freedom for estimating the variability in this model (neglecting autocorrelation; see below).

The response patterns shown earlier in Figure 3 are scaled by natural variability to create Figure 6, expressing the projected change in units of the number of standard deviations of interannual variability at each location

Table 1
Years From Start of Deployment Until the Signal-to-Noise Ratio for Precipitation Averaged Over Land, Ocean, and Globally Meets a Threshold of Either One (Before Brackets) or Two (Within Brackets) for Different Scenarios and Different Target Temperatures

| Scenario	RCP4.5		RCP8.5	
Target (°C)	1.5	2	1.5	2
Land-average	25 (44)	30 (45)	21 (31)	16 (28)
Ocean-average	8 (15)	10 (11)	7 (10)	7 (9)
Global	7 (11)	8 (11)	6 (9)	5 (9)
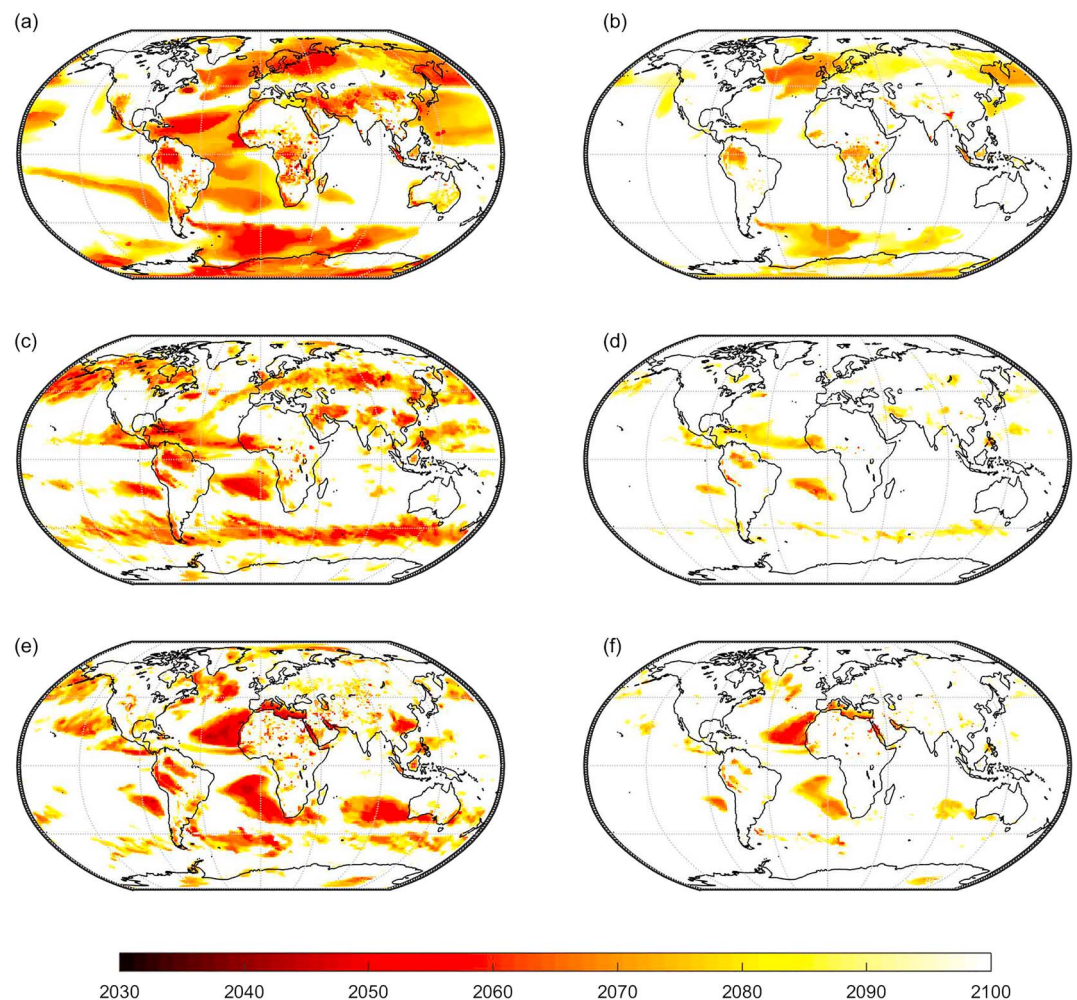
Figure 7. Detection timescale for an RCP4.5 scenario in which stratospheric aerosol geoengineering is used to maintain global mean temperature at 1.5 °C; in this model the start of deployment is in 2027 with a gradual increase in forcing (see Figure 2b). The time is calculated as the first year in which the magnitude of the projected change is larger than one (panels a, c, e) or two (b, d, f) standard deviations of the variability in estimating that change from observations (using equation (6)). Results are shown for (a, b) temperature, (c, d) precipitation, and (e, f) P − E. Results for different scenarios are shown in the supporting information.

per degree of cooling provided by the geoengineering. For temperature, for example, high-latitude variability tends to be larger than in the tropics, and so Figure 6 shows more emphasis on tropical regions than Figure 3. For each 1 °C change (an increase in GHG offset by an increase in geoengineering), 7.5%, 2%, and 3% of the land area is projected to have changes in temperature, precipitation, and P − E, respectively, above 0.25 standard deviations, and almost none have changes above 0.5 standard deviations (the cumulative fraction of land area with changes above a given threshold is shown in Figure S4).

4.2. Detection

If geoengineering were abruptly initiated with a constant cooling level, and autocorrelation in the natural variability were ignored, then the timescale for detection could be obtained directly from Figure 6 by finding the year N where $\sqrt{N}$ times the response equalled some threshold. However, scenarios for geoengineering deployment such as in Figure 2b involve only gradually increasing the forcing over time. Furthermore, because natural variability has some interannual autocorrelation, the variance after averaging over N years typically falls off more slowly than $1/N$, although this can also be influenced by the feedback algorithm used in the GLENS simulations (see Figure S4 for an illustration). The calculation of detection time therefore requires slightly more complication than a straightforward $\sqrt{N}$ scaling.
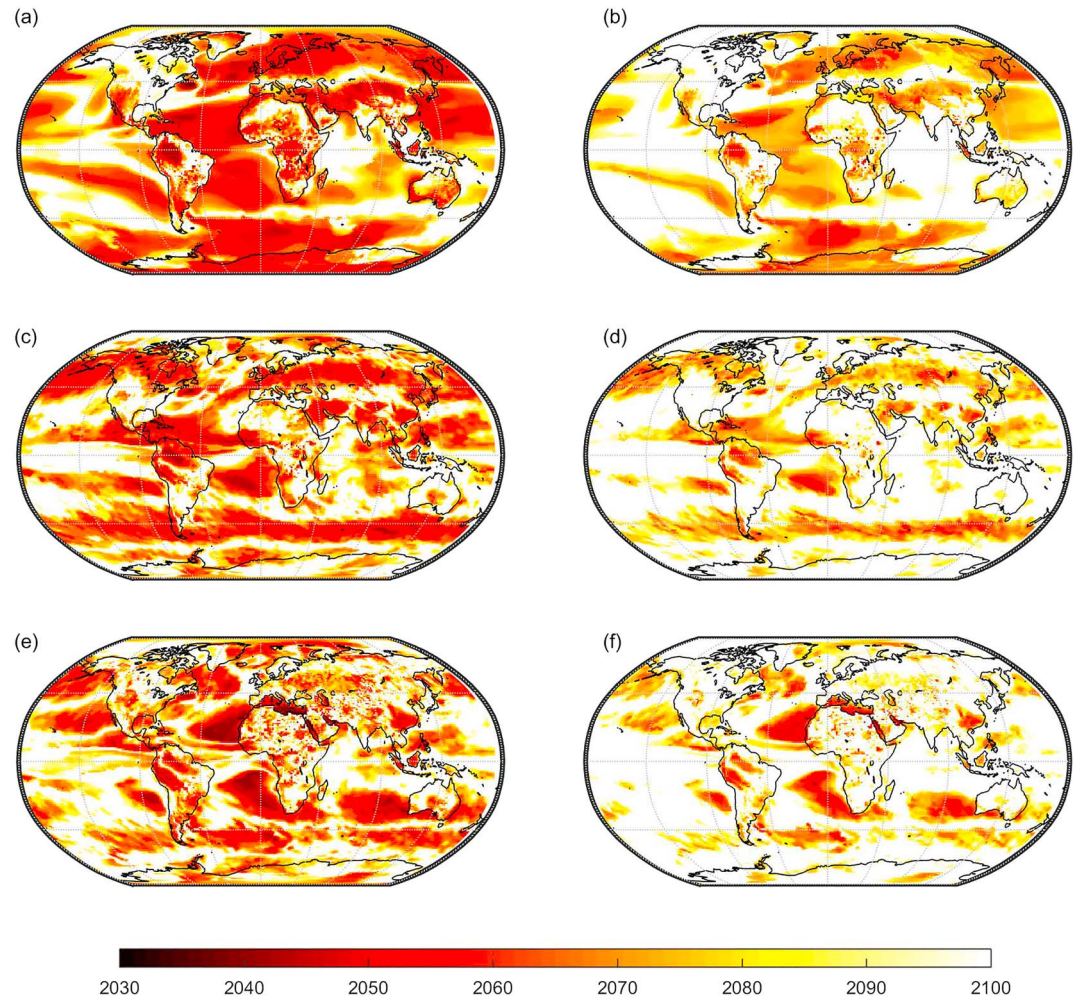
Figure 8. Detection timescale for an RCP8.5 scenario in which stratospheric aerosol geoengineering is used to maintain global mean temperature at 1.5 °C; similar to Figure 7 except for the high forcing scenario. Time to reach a signal-to-noise ratio threshold of one (a, c, e) or two (b, d, f) for temperature (a, b), precipitation (c, d) and P − E (e, f).

Suppose the amount of geoengineering during a deployment changed with time according to the function $u(t)$, which we can measure in units of degrees Celsius of cooling as in Figure 2b. Then assuming pattern scaling, the change in any variable $y(t)$ during the deployment is given by $y(t) = \beta u(t) + n(t)$, where β is the response per degree, for example, from Figure 3, and $n(t)$ captures the effects of climate variability and any zero-mean uncertainty in the observations themselves. Any unknown constant bias in the observation system will have no effect as we are concerned only with changes in y. If an observer were trying to estimate the value of β from observations of $y(t)$ over the interval from time t_0 to t_f, the best estimate would be given by the projection

$$\hat{\beta} = \int_{t_0}^{t_f} y(t)u(t)dt \div \int_{t_0}^{t_f} u(t)u(t)dt \qquad (5)$$

and the noise corrupting this estimate would be given by

$$\eta = \int_{t_0}^{t_f} n(t)u(t)dt \div \int_{t_0}^{t_f} u(t)u(t)dt. \qquad (6)$$

The signal-to-noise ratio (SNR) after time $\Delta t = t_f - t_0$ is thus β divided by the standard deviation of η. To test for statistical significance at a 95% confidence level would require an SNR larger than roughly two, while an SNR of one gives roughly two-thirds confidence of a change (both assuming a two-sided test with sufficient degrees of freedom). The signal we obtained in section 3, and the noise statistics we can also estimate from
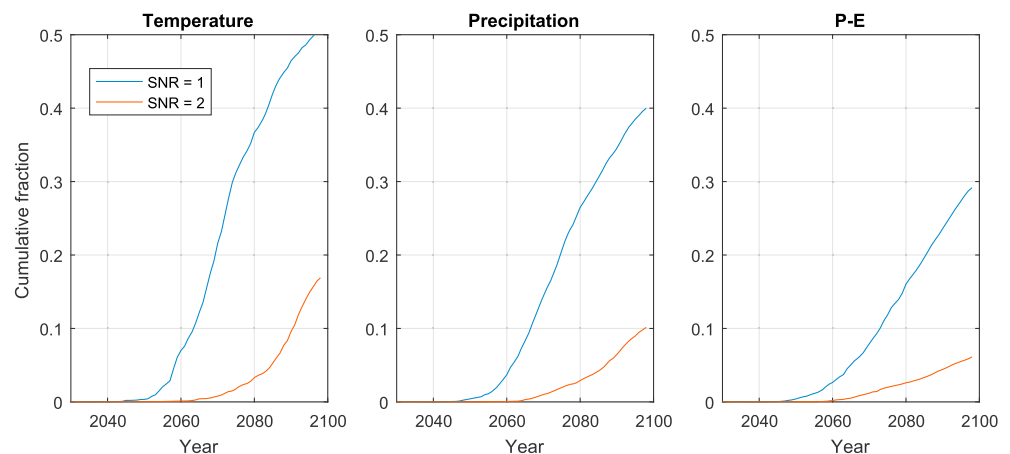
Figure 9. Cumulative fraction of land area reaching an SNR threshold of one (blue) or two (red) as a function of time, for an RCP4.5 scenario with a 1.5 °C target as shown in Figure 7. Temperature (left), precipitation (center), and P − E (right). SNR = signal-to-noise ratio.

our ensemble of simulations. We compute η and its standard deviation using the 20-member ensemble of geoengineering simulations, rather than the RCP8.5 simulations without geoengineering, in order to obtain statistics through to 2099 with 20 rather than only 3 ensemble members.

As noted earlier, the feedback algorithm influences variability in the controlled degrees of freedom (MacMartin et al., 2014). By suppressing global-scale temperature variability at long timescales, the feedback algorithm might also be reducing long timescale variability at a regional scale, which could make detection slightly easier for an observer relative to a deployment in which the injection rates were not adjusted based on observations. The three-member RCP8.5 ensemble without geoengineering is not large enough to clearly evaluate this hypothesis (suggesting that it is at most a small effect); see, for example, Figure S5.

The change in global mean precipitation based on the GLENS simulations has an SNR greater than one for any of the scenarios shown in Figure 2b after 5–8 years and SNR greater than two after 9–11 years; see Table 1. Most of the change in precipitation in these simulations occurs over the ocean, and thus the corresponding detection times for land-average precipitation are considerably longer. If we had chosen a scenario in which global mean precipitation were held constant rather than global mean temperature, then the change in global mean precipitation would be undetectable by definition, but the change in global mean temperature would be detectable in a time-frame comparable to those in Table 1.

The changes at the model grid-scale take longer to detect. These are shown in Figures 7 and 8, for an RCP4.5 or RCP8.5 scenario, respectively, in which geoengineering is used to maintain global mean temperature at 1.5 °C; the cases for a 2 °C target are shown in Figures S6–S7. For the more limited deployment scenario where emissions follow an RCP4.5 trajectory, the fraction of land area over which changes are projected to be detectable by a given year are shown in Figure 9. By the end of the century, only 10% of the land area is projected to reach an SNR of two for precipitation changes, and only 6% for detecting P − E changes. Using much larger amounts of geoengineering to maintain constant temperature while following the higher emissions RCP8.5 scenario will result in more rapidly detectable climate changes: changes in P − E, for example, reach an SNR of two over 35% of the land area by the end of the century.

Recall that these describe the timescale for detecting changes relative to the case with the same global mean temperature but no geoengineering. The differences between the geoengineered case and one without geoengineering where the global mean temperature was continuing to increase would be much larger and more rapidly detectable (as in Bürger & Cubasch, 2015; Lo et al., 2016).

Local spatial averaging does not substantially improve detectability. This is illustrated for precipitation changes in Figure S8 where a moving area-weighted averaging window is applied in both latitude and longitude prior to conducting analysis. Averaging spatially reduces the variability (due to spatial decorrelation), but it also roughly comparably reduces the amplitude of the signal, leading to relatively minor

impact on detection timescales. An alternate illustration of this effect is shown in Figure S9 where the spatial averaging is instead performed over Giorgi regions (Giorgi & Francisco, 2000). At a sufficiently large-scale, precipitation changes become more detectable as the signal becomes dominated by the reduction in global-mean precipitation rather than by regional increases and decreases.

The analysis above focused only on annual-mean changes in temperature, precipitation, and P − E. Detection timescales are similar for changes averaged only over winter or summer months (Figures S10 and S11). A similar analysis could also be conducted for other variables. One variable that would be detectable at a grid-scale in less than a decade is changes in aerosol optical depth (assuming appropriate observational systems were in place).

5. Discussion and Conclusions

This paper considers the pattern of climate response induced by stratospheric sulfate aerosol geoengineering, compares the magnitude of these changes with the magnitude of natural variability, and for different future scenarios considers the time it would take for these changes to emerge from the background natural climate variability—how long it would take based on observations to detect a change with an SNR exceeding a threshold of one, or of two (yielding roughly two-thirds or 95% confidence, respectively, in detecting a change). Geoengineering would not affect the climate in the same way as atmospheric GHG concentrations, and these analyses provide useful inputs into understanding how important the projected differences in response might be.

We use an ensemble of climate model simulations to better distinguish the forced response from natural variability. These simulations were conducted in a climate model that simultaneously includes many important physical processes, including aerosol microphysics, interactive stratospheric chemistry, and stratospheric dynamics, as well as coupling with land, sea ice, and ocean models.

Because the impacts of stratospheric aerosol geoengineering would depend on how it is deployed, the response should ideally be considered using simulations that make deliberate choices. The simulations used herein inject SO_2 into the stratosphere at four different latitudes rather than only one in order to better compensate for the pattern of warming due to increased GHG concentrations and reduce the magnitude of residual climate differences. There remains considerable scope for improving on this strategy, and the results of these geoengineering simulations should not be interpreted as conclusions about unavoidable impacts of any possible geoengineering deployment.

Despite that caveat, we find that projected regional differences between, for example, an RCP4.5 scenario of GHG emissions with sufficient stratospheric aerosols to maintain a 1.5 °C global mean temperature, and a world with the same global mean temperature and lower GHG, are relatively small. For example, in this scenario, estimating the magnitude of the shift in global mean precipitation in the presence of natural variability would reach an SNR of one after 7 years, while this threshold is not reached for precipitation changes at a grid-scale by the end of the century in most locations; similar results hold for P − E. Changes in temperature typically have shorter detection timescales than precipitation or P − E, although at a grid-scale only 50% of the land area would reach an SNR of one by the end of the century.

The changes are (to first order) proportional to the amount of geoengineered cooling. One reason why the projected changes are difficult to detect in this scenario is that only 1.7 °C of cooling is being provided by the end of the century. If there is less mitigation and correspondingly larger deployment of geoengineering, then the differences with respect to a climate with low GHG and the same global mean temperature become more significant, and would be more readily detected before the end of the century.

While this type of information may be useful to provide better context for the magnitude of current model-projected climate changes with stratospheric aerosol geoengineering, current knowledge remains insufficient for informed decisions. There are many uncertainties in this and any climate model (e.g., MacMartin et al., 2016), and it would be valuable to conduct similar simulations in other climate models to better assess the robustness of projected changes. There are also many more relevant variables than the few selected for analysis herein. Finally, just because a shift in the mean is difficult to detect in the presence of variability does not necessarily guarantee that shift is unimportant.

References

Aquila, V., Garfinkel, C. I., Newman, P. A., Oman, L. D., & Waugh, D. W. (2014). Modifications of the quasi-biennial oscillation by a geoengineering perturbation of the stratospheric aerosol layer. *Geophysical Research Letters*, *41*, 1738–1744. https://doi.org/10.1002/2013GL058818

Benduhn, F., Schallock, J., & Lawrence, M. G. (2016). Early growth dynamical implications for the steerability of stratospheric solar radiation management via sulfur aerosol particles. *Geophysical Research Letters*, *43*, 9956–9963. https://doi.org/10.1002/2016GL070701

Bürger, G., & Cubasch, U. (2015). The detectability of climate engineering. *Journal of Geophysical Research: Atmospheres*, *120*, 11,404–11,418. https://doi.org/10.1002/2015JD023954

Caldeira, K., & Myhrvold, N. (2013). Projections of the pace of warming following an abrupt increase in atmospheric carbon dioxide concentration. *Environmental Research Letters*, *8*(3), 034039.

Castruccio, S., McInerney, D. J., Stein, M. L., Crouch, F. L., Jacob, R. L., & Moyer, E. J. (2014). Statistical emulation of climate model projections based on precomputed GCM Runs. *Journal of Climate*, *27*, 1829–1844.

Crutzen, P. J. (2006). Albedo enhancement by stratospheric sulfur injections: A contribution to resolve a policy dilemma? *Climatic Change*, *77*, 211–219. https://doi.org/10.1007/s10584-006-9101-y

Dai, Z., Weisenstein, D., & Keith, D. W. (2018). Tailoring meridional and seasonal radiative forcing by sulfate aerosol solar geoengineering. *Geophysical Research Letters*, *45*, 1030–1039. https://doi.org/10.1002/2017GL076472

Deser, C., Phillips, A., Bourdette, V., & Teng, H. (2012). Uncertainty in climate change projections: The role of internal variability. *Climate Dynamics*, *38*, 527–546. https://doi.org/10.1007/s00382-010-0977-x

Driscoll, S., Bozzo, A., Gray, L. J., Robock, A., & Stenchikov, G. (2012). Coupled Model Intercomparison Project 5 (CMIP5) simulations of climate following volcanic eruptions. *Journal of Geophysical Research*, *117*, D17105. https://doi.org/10.1029/2012JD017607

English, J. M., Toon, O. B., & Mills, M. J. (2012). Microphysical simulations of sulfur burdens from stratospheric sulfur geoengineering. *Atmospheric Chemistry and Physics*, *12*(10), 4775–4793.

Fasullo, J. T., Tilmes, S., Richter, J. H., Kravitz, B., MacMartin, D. G., Mills, M. J., & Simpson, I. R. (2018). Persistent polar ocean warming in a strategically geoengineered climate. *Nature Geoscience*, *11*, 910–914. https://doi.org/10.1038/s41561-018-0249-7

Frame, D., Joshi, M., Hawkins, E., Harrington, L. J., & de Roiste, M. (2017). Population-based emergence of unfamiliar climates. *Nature Climate Change*, *7*, 407–412. https://doi.org/10.1038/NCLIMATE3297

Giorgi, F., & Francisco, R. (2000). Uncertainties in regional climate change prediction: A regional analysis of ensemble simulations with the HADCM2 coupled AOGCM. *Climate Dynamics*, *16*, 169–182.

Hawkins, E., & Sutton, R. (2012). Time of emergence of climate signals. *Geophysical Research Letters*, *39*, L01702. https://doi.org/10.1029/2011GL050087

Haywood, J. M., Jones, A., Bellouin, N., & Stephenson, D. (2013). Asymmetric forcing from stratospheric aerosols impacts Sahelian rainfall. *Nature Climate Change*, *3*, 660–665. https://doi.org/10.1038/nclimate1857

Heckendorn, P., Weisenstein, D., Fueglistaler, S., Luo, B. P., Rozanov, E., Schraner, M., et al. (2009). The impact of geoengineering aerosols on stratospheric temperature and ozone. *Environmental Research Letters*, *4*(4), 045108.

Holden, P. B., & Edwards, N. R. (2010). Dimensionally reduced emulation of an AOGCM for application to integrated assessment modelling. *Geophysical Research Letters*, *37*, L21707. https://doi.org/10.1029/2010GL045137

Intergovernmental panel on climate change (IPCC) (2018). *Global warming of 1.5° C, an IPCC special report on the impacts of global warming of 1.5° C above pre-industrial levels and related global greenhouse gas emission pathways, in the context of strengthening the global response to the threat of climate change, sustainable development, and efforts to eradicate poverty*. Geneva, Switzerland: IPCC.

Jones, A. C., Hawcroft, M. K., Haywood, J. M., Jones, A., Guo, X., & Moore, J. C. (2018). Regional climate impacts of stabilizing global warming at 1.5 K using solar geoengineering. *Earth's Future*, *6*, 230–251. https://doi.org/10.1002/2017EF00720

Joshi, M. M., Turner, A. G., & Hope, C. (2013). The use of land-sea warming contrast under climate change to improve impact metrics. *Climate Change*, *117*(4), 951–960.

Kalidindi, S., Bala, G., Modak, A., & Caldeira, K. (2015). Modeling of solar radiation management: A comparison of simulations using reduced solar constant and stratospheric sulphate aerosols. *Climate Dynamics*, *44*(9), 2909–2925. https://doi.org/10.1007/s00382-014-2240-3

Kay, J. E., Deser, C., Phillips, A., Mai, A., Hannay, C., Strand, G., et al. (2015). The community earth system model (CESM) large ensemble project: A community resource for studying climate change in the presence of internal climate variability. *Bulletin of the American Meteorological Society*, *96*(8), 1333–1349. https://doi.org/10.1175/BAMS-D-13-00255.1

Keith, D. W., & Irvine, P. J. (2016). Solar geoengineering could substantially reduce climate risks – A research hypothesis for the next decade. *Earth's Future*, *4*, 549–559. https://doi.org/10.1002/2016EF000465

Keith, D. W., & MacMartin, D. G. (2015). A temporary, moderate and responsive scenario for solar geoengineering. *Nature Climate Change*, *5*, 201–206. https://doi.org/10.1038/nclimate2493

Keith, D. W., Weisenstein, K. K., Dykema, J. A., & Keutsch, F. N. (2016). Stratospheric solar geoengineering without ozone loss? *Proceedings of the National Academy of Sciences of the United States of America*, *113*(52), 14,910–14,914.

Kleinschmitt, C., Boucher, O., & Platt, U. (2018). Sensitivity of the radiative forcing by stratospheric sulfur geoengineering to the amount and strategy of the SO_2 injection studied with the LMDZ-S3A model. *Atmospheric Chemistry and Physics*, *18*, 2769–2786. https://doi.org/10.5194/acp-18-2769-2018

Kravitz, B., Caldeira, K., Boucher, O., Robock, A., Rasch, P. J., Alterskjær, K., et al. (2013). Climate model response from the geoengineering model intercomparison project (GeoMIP). *Journal of Geophysical Research: Atmospheres*, *118*, 8320–8332. https://doi.org/10.1002/JGRD.50646

Kravitz, B., MacMartin, D. G., Mills, M. J., Richter, J. H., Tilmes, S., Lamarque, J. F., et al. (2017). First simulations of designing stratospheric sulfate aerosol geoengineering to meet multiple simultaneous climate objectives. *Journal of Geophysical Research: Atmospheres*, *122*, 12,616–12,634. https://doi.org/10.1002/2017JD026874

Kravitz, B., MacMartin, D. G., Robock, A., Rasch, P. J., Ricke, K. L., Cole, J. N. S., et al. (2014). A multi-model assessment of regional climate disparities caused by solar geoengineering. *Environmental Research Letters*, *9*(7), 074013. https://doi.org/10.1088/1748-9326/9/7/074013

Kravitz, B., MacMartin, D. G., Wang, H., & Rasch, P. J. (2016). Geoengineering as a design problem. *Earth Systems Dynamics*, *7*, 469–497. https://doi.org/10.5194/esd-7-469-2016

Liu, X., Easter, R. C., Ghan, S. J., Zaveri, R. A., Rasch, P. J., Shi, X., et al. (2012). Toward a minimal representation of aerosols in climate models: Description and evaluation in the community atmosphere model CAM5. *Geoscientific Model Development*, *5*(3), 709–739. https://doi.org/10.5194/gmd-5-709-2012

Lo, Y. T. E., Charlton-Perez, A. J., Lott, F. C., & Highwood, E. J. (2016). Detecting sulphate aerosol geoengineering with different methods. *Scientific Reports*, *6*, 39169. https://doi.org/10.1038/srep39169

Long, J. C. S., & Shepherd, J. G. (2014). The strategic value of geoengineering research. In B. Freedman (Eds), *Global Environmental Change. Handbook of Global Environmental Pollution* (Vol 1). Dordrecht: Springer.

MacMartin, D. G., & Kravitz, B. (2016). Dynamic climate emulator for solar geoengineering. *Atmospheric Chemistry and Physics*, *16*, 15789–15799. https://doi.org/10.5194/acp-16-15789-2016

MacMartin, D. G., Kravitz, B., Keith, D. W., & Jarvis, A. J. (2014). Dynamics of the coupled human-climate system resulting from closed-loop control of solar geoengineering. *Climate Dynamics*, *43*(1–2), 243–258.

MacMartin, D. G., Kravitz, B., Long, J. C. S., & Rasch, P. J. (2016). Geoengineering with stratospheric aerosols: What don't we know after a decade of research? *Earth's Future*, *4*, 543–548. https://doi.org/10.1002/2016EF000418

MacMartin, D. G., Kravitz, B., Tilmes, S., Richter, J. H., Mills, M. J., Lamarque, J. F., et al. (2017). The climate response to stratospheric aerosol geoengineering can be tailored using multiple injection locations. *Journal of Geophysical Research: Atmospheres*, *122*, 12,574–12,590. https://doi.org/10.1002/2017JD026868

MacMartin, D. G., Ricke, K. L., & Keith, D. W. (2018). Solar geoengineering as part of an overall strategy for meeting the 1.5°C Paris target. *Philosophical Transactions of the Royal Society A*, *376*, 20160454. https://doi.org/10.1098/rsta.2016.0454

MacMynowski, D. G., Shin, H. J., & Caldeira, K. (2011). The frequency response of temperature and precipitation in a climate model. *Geophysical Research Letters*, *38*, L16711. https://doi.org/10.1029/2011GL048623

Meinshausen, M., Smith, S. J., Calvin, K. V., Daniel, J. S., Kainuma, M. L. T., Lamarque, J. F., et al. (2011). The RCP greenhouse gas concentrations and their extension from 1765 to 2300. *Climatic Change*, *109*, 213–241. https://doi.org/10.1007/s10584-011-0156-z

Mills, M., Richter, J. H., Tilmes, S., Kravitz, B., MacMartin, D. G., Glanville, A. A., et al. (2017). Radiative and chemical response to interactive stratospheric aerosols in fully coupled CESM1(WACCM). *Journal of Geophysical Research: Atmospheres*, *122*, 13,061–13,078. https://doi.org/10.1002/2017JD027006

Mills, M. J., Schmidt, A., Easter, R., Solomon, S., Kinnison, D. E., Ghan, S. J., et al. (2016). Global volcanic aerosol properties derived from emissions, 1990–2014, using CESM1(WACCM). *Journal of Geophysical Research: Atmospheres*, *121*, 2332–2348. https://doi.org/10.1175/JCLI-D-12-00558.1

Mitchell, T. D. (2003). Pattern scaling: An examination of the accuracy of the technique for describing future climates. *Climatic Change*, *60*, 217–242.

Niemeier, U., & Timmreck, C. (2015). What is the limit of climate engineering by stratospheric injection of SO_2? *Atmospheric Chemistry and Physics*, *15*, 9129–9141.

Pierce, J. R., Weisenstein, D. K., Heckendorn, P., Peter, T., & Keith, D. W. (2010). Efficient formation of stratospheric aerosol for climate engineering by emission of condensible vapor from aircraft. *Geophysical Research Letters*, *37*, L18805. https://doi.org/10.1029/2010GL043975

Pitari, G., Aquila, V., Kravitz, B., Robock, A., Watanabe, S., Cionni, I., et al. (2014). Stratospheric ozone response to sulfate geoengineering: Results from the geoengineering model intercomparison project (GeoMIP). *Journal of Geophysical Research: Atmospheres*, *119*, 2629–2653. https://doi.org/10.1002/2013JD020566

Richter, J. H., Tilmes, S., Glanville, A., Kravitz, B., MacMartin, D. G., Mills, M. J., et al. (2018). Stratospheric response in the first geoengineering simulation meeting multiple surface climate objectives. *Journal of Geophysical Research: Atmospheres*, *123*, 5762–5782. https://doi.org/10.1029/2018JD028285

Richter, J. H., Tilmes, S., Mills, M. J., Tribbia, J. J., Kravitz, B., MacMartin, D. G., et al. (2017). Stratospheric dynamical response and ozone feedbacks in the presence of SO_2 injection. *Journal of Geophysical Research: Atmospheres*, *122*, 12,557–12,573. https://doi.org/10.1002/2017JD026912

Ricke, K. L., Granger Morgan, M., & Allen, M. R. (2010). Regional climate response to solar-radiation management. *Nature Geoscience*, *3*, 537–541. https://doi.org/10.1038/NGEO915

Rogelj, J., den Elzen, M., Höhne, N., Fransen, T., Fekete, H., Winkler, H., et al. (2016). Paris agreement climate proposals need a boost to keep warming well below 2° C. *Nature*, *534*, 631–639. https://doi.org/10.1038/nature18307

Santer, B. D., Wigley, T. M. L., Schlesinger, M. E., & Mitchell, J. F. B. (1990). Developing climate scenarios from equilibrium GCM results (*MPI Report Number 47*). Hamburg, Germany.

Tebaldi, C., & Arblaster, J. M. (2014). Pattern scaling: Its strengths and limitations, and an update on the latest model simulations. *Climatic Change*, *122*, 459–471.

Tilmes, S., Richter, J. H., Kravitz, B., MacMartin, D. G., Mills, M. J., Simpson, I., et al. (2018). CESM1(WACCM) stratospheric aerosol geoengineering large ensemble (GLENS) project. *Bulletin of the American Meteorological Society*, *99*, 2361–2371. https://doi.org/10.1175/BAMS-D-17-0267.1

Tilmes, S., Richter, J. H., Mills, M. M., Kravitz, B., MacMartin, D. G., Garcia, R. R., et al. (2018). Effects of different stratospheric SO_2 injection altitude on stratospheric chemistry and dynamics. *Journal of Geophysical Research: Atmospheres*, *123*, 4654–4673. https://doi.org/10.1002/2017JD028146

Tilmes, S., Richter, J. H., Mills, M. J., Kravitz, B., MacMartin, D. G., Vitt, F., et al. (2017). Sensitivity of aerosol distribution and climate response to stratospheric SO_2 injection locations. *Journal of Geophysical Research: Atmospheres*, *122*, 12,591–12,615. https://doi.org/10.1002/2017JD026888

Wigley, T. M. L. (2006). A combined mitigation/geoengineering approach to climate stabilization. *Science*, *314*, 452–454.